GEOPHYSICS, VOL. 75, NO. 3 (MAY-JUNE 2010); P. MA1–MA7, 10 FIGS., 1 TABLE.
10.1190/1.3377789

A comparison of passive seismic monitoring of fracture stimulation from water and CO_2 injection

James P. Verdon[1], J.-Michael Kendall[1], and Shawn C. Maxwell[2]

ABSTRACT

Hydraulic fracturing is used to create pathways for fluid migration and to stimulate production. Usually, water is the injected fluid, although alternative fluids such as carbon dioxide (CO_2) have been used recently. The amount of fracturing that CO_2 can induce is also of interest for the security of carbon capture and storage. Hydraulic fracturing is usually monitored using passive seismic arrays, detecting microseismic events generated by the fracturing. It is of interest to compare the amount of seismicity that CO_2 injection can generate in comparison with water. With this in mind, we have analyzed a passive seismic data set monitoring the injection of water and supercritical CO_2 under very similar conditions, allowing us to make a direct comparison between the fluids. We examined event locations and event magnitudes, and we used shear-wave splitting to image the fractures that are generated. For both fluids,the event locations map the formation of fractures moving away from the injection well with normals parallel to the minimum principal stress. The events during water injection are limited to the injection depth, while during CO_2 injection, activity migrates above the injection depth. Event magnitudes are similar in both cases, and larger event magnitudes appear to correlate with higher injection pressures. Shear-wave splitting suggests that water injection generates more fractures, though the data quality is not good enough to make a robust conclusion about this. The comparability between water and CO_2 injection means that lessons can be learned from the abundant experience of conventional water injection.

INTRODUCTION

Hydraulic fracturing provides a tool that increases the permeability of a reservoir, stimulating increased production. Water and water-based gels have been the main fluids injected to generate hydraulic fracturing. However, other fluids such as steam and carbon dioxide (CO_2) are increasingly being used to stimulate production. CO_2 is also being injected into some reservoirs (most notably Weyburn and Sleipner) for storage purposes. In this paper, we compare the results of passive seismic monitoring of CO_2 and water injection to evaluate the fluids' effectiveness at inducing fractures.

Hydraulic fracturing is commonly monitored using passive seismic techniques. By placing geophones downhole in or near the reservoir, it is possible to detect microseismic events generated by fracturing. Many of the techniques used to analyze the recorded data are derived from global earthquake seismology. Analysis of event locations (e.g., De Meersman et al., 2006), focal mechanisms and magnitudes (e.g., Rutledge et al., 2004), and wave-propagation effects such as shear-wave splitting (e.g., Teanby et al., 2004a) can provide information about the stress state in the reservoir, pressure fronts induced by injection, and the geometry and intensity of fracturing in and around the reservoir. The use of passive seismic monitoring has developed rapidly over the previous 15–20 years.

It is unclear whether CO_2 injection should induce the same rates, patterns, and magnitudes of seismicity as water injection. The lower density of CO_2 in comparison to water may lead to density-driven stress changes, causing different patterns of seismicity (e.g., Minchak et al., 2002). Supercritical CO_2 has a bulk modulus at least one order of magnitude smaller than water, and some workers have suggested that, because CO_2 has a higher compressibility, it represents a softer hammer than other injection fluids. As such, it will have inherently lower seismic deformation efficiency (see Maxwell et al. [2008] for a discussion of seismic deformation efficiency). Furthermore, depending on the fluid initially present in the pore space, there may be relative permeability differences between the fluids. This

Manuscript received by the Editor 19 March 2009; revised manuscript received 28 July 2009; published online 22 April 2010.
[1]University of Bristol, Department of Earth Sciences, Bristol, U. K. E-mail: gljpv@bris.ac.uk; gljmk@bris.ac.uk.
[2]Schlumberger Canada Ltd., Calgary, Alberta, Canada. E-mail: smaxwell@calgary.oilfield.slb.com.

would influence the injectivity and therefore, presumably, the amount of fracturing induced.

As a result, there is still significant uncertainty as to the amount of fracturing and seismicity to expect when injecting CO_2. This is an issue not just for hydraulic fracturing but also for carbon capture and storage (CCS), where CO_2 is captured at power stations and injected into mature hydrocarbon reservoirs. There is still much debate about the best ways to monitor this process, but passive seismic monitoring has been deployed at the Weyburn CCS pilot project (for details, see White, 2008). The amount of fracturing that CO_2 injection could generate is of great interest within the CCS community because this will directly influence reservoir integrity. Furthermore, the magnitude of event that CO_2 injection can generate will determine the feasibility of induced-microseismic-event detection to be used as a monitoring tool for CCS.

We endeavor to make a direct empirical comparison between CO_2 and water injection. We have analyzed a data set where CO_2 and water have been injected into an oil field to induce hydraulic fracturing. To make the comparison as fair as possible, both fluids have been injected at similar rates, with similar injection pressures, into the same reservoir. Both stages have been monitored on the same downhole geophone array. We aim to use this data set to image the orientation and extent of the fracturing and to use event magnitudes and shear-wave-splitting analysis to place bounds on the amount of fracturing caused by injecting the different fluids. This will allow us to consider the deformation efficiency of CO_2 compared to other fluids.

Field background and description

A hydraulic fracture job was performed in a North American producing oilfield to create and improve pathways for fluid migration and to stimulate production. Owing to confidentiality agreements, information about the geology and history of this field is limited.

The thick reservoir contains potential barriers to vertical flow. Therefore, to ensure fracturing throughout the reservoir thickness, nine stages of fracturing were conducted from one vertical well extending through the reservoir, beginning at its base and moving upward. For the first seven stages, a water-based gel (hereafter referred to as water, for brevity) was used as the injection fluid. However, supercritical CO_2 was used for the final two stages. The motivation for this was to test the effectiveness of hydraulic fracturing with different fluids.

We have available data from one water injection stage and one CO_2 injection stage conducted one month later. No major lithologic differences have been identified between the two fracture depths, so any differences in observed seismicity can be attributed to the different injection fluids. To monitor the fracturing, 12 three-component geophones spaced at 12-m intervals were installed in a vertical observation well a short distance from the injection well. For each stage, the geophones were moved such that most of the recorded waves traveled subhorizontally through the reservoir. The locations of the injection depths and recording geophones for the two stages are plotted in Figure 1.

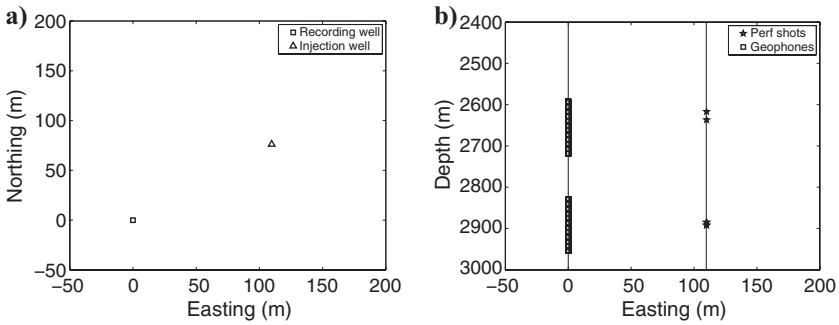

Figure 1. (a) Map view and (b) cross-section plots, showing injection depths and recording geophones for both stages of fracturing. The upper shots and receivers in (b) are for the CO_2 injection stage; the lower shots and receivers are the water stage.

EVENT LOCATIONS

To locate the microseismic events, a 1D isotropic layered velocity model was generated using sonic-log information. Events were considered as reliable when orthogonally polarized P- and S-waves could be identified as arriving in a consistent manner across at least two geophones in the array. Of the hundreds of potential triggers recorded by the automated triggering mechanism, approximately 50–100 for each stage were found to be reliable microseismic events. Event locations were computed using P-wave particle motion for azimuth and P-/S-wave traveltime differences for distance. Arrival-time shifts across the geophone array were combined with ray tracing through the velocity model to compute event elevation. The quality of event location was assessed using the method of Zimmer et al. (2007).

Water injection

The water-injection stage that we consider was initiated by perforation shots that penetrated the well at depths between 2885 and 2892 m. Water was injected at high pressures, and microseismic activity was recorded immediately upon injection. Injection continued for approximately 80 minutes, and microseismic events were recorded throughout and for a short period after injection. Figure 2 shows in detail the injection pressure (at surface) and fluid-flow rates as well as the rate of microseismic activity. In total, 65 events were reliably identified and located.

Figure 3 shows the locations of the events. The error bars plotted represent the one-standard-deviation errors computed from the variation in P-wave partical motion across the array and residuals between predicted and picked traveltimes. These errors are low. However, they do not account for potential errors in the velocity model used to compute event locations (e.g., Eisner et al., 2009). These may be introduced in a number of ways: anisotropy (which we know to be present from shear-wave-splitting observations), lateral heterogeneity, and upscaling sonic logs to seismic velocities. The errors introduced by having a simplified velocity model (i.e., 1D, isotropic) are much harder to quantify, so the errors plotted here must be considered a lower bound for the actual errors.

The events extend from the injection well to the northwest and southeast with a strike of ~120°; in cross section, the events are restricted in vertical extent, occurring close to the depth of perforation. The containment of the microseismicity to a narrow band at the injection depth may indicate containment of the elevated pressures by sedimentary structures. However, without further

knowledge of the geology of the reservoir, it is difficult to comment on why this might be the case.

The events extending in a linear fashion from the injection well image the growth of fractures with a northwest-southeast orientation. Assuming that the maximum principal stress is subvertical, we deduce that the minimum principal stress is horizontal, trending northeast-southwest. From the lateral extent of microseismic activity, we observe fractures extending at least 125 m to the northwest and 80 m to the southeast of the injection well — a total distance of 205 m.

CO_2 injection

CO_2 injection was initiated one month after the water-injection stage. The injection well was perforated between 2617 and 2637 m, and supercritical CO_2 was used as the injection fluid. Again, microseismic activity was recorded for the duration of injection. The injection rates and pressures are plotted in Figure 4 along with the microseismicity rate.

Figure 5 shows the event locations during CO_2 injection. In map view, the locations show a similar pattern to the water-injection events, extending to the northwest and southeast of the injection well at approximately 120°, imaging the formation of vertical fractures with this strike. However, the events migrate well above the injection depth during CO_2 injection. It is certainly possible that this increased vertical extent is a result of the increased buoyancy and mobility of CO_2 in comparison to water. However, without more detailed knowledge of the reservoir, it is impossible to rule out the presence of higher-permeability pathways (such as pre-existing fractures) or stress barriers above this depth that could also generate this observation. The events during CO_2 injection extend 65 m to the northwest and 50 m to the southeast — a total of 115 m — which is less than that observed for water injection.

The injection pressures and rates are similar for both stages, as are the rates of microseismicity. Fifty events were recorded during 63 minutes of CO_2 injection (or 1.26 minutes per event), in comparison with 65 during water injection (at 1.2 minutes per event). Furthermore, the maximum rates of seismicity in Figures 2 and 4 are similar, with at most 13 events in 5 minutes during water injection and 14 events in 5 minutes during CO_2 injection.

EVENT MAGNITUDES

To compare the intensity of fracturing caused by injecting the two different fluids, we analyze the magnitudes of events recorded during the two stages. Figure 6 plots the injection pressures and event magnitudes during both stages; the scales in both plots are equal. Event magnitudes are similar for both stages, with most events having magnitudes between −3.6 and −3.2. For both stages, there appears to be correlation between injection pressure and event magnitude. Note, for example, that the drop in injection pressure between 16 and 22 minutes during water injection correlates with a drop in event magnitude. During CO_2 injection, the initial stepped increase in injection pressures matches the stepped increase in event magnitude.

This correlation between injection pressure and event magnitude can be tested more directly by computing the correlation coefficient between magnitude and injection pressure at the time the event occurs. The statistical significance of the correlations is computed with a t-test, with the null hypothesis that there is no correlation. We consider the water and CO_2 cases separately. If the magnitudes are independent of fluid properties, then combining the data sets should produce correlation. Therefore, we also compute correlation for all of the data points together. The correlation coefficients and statistical significance of correlation are given in Table 1.

In Figure 7, we plot the event magnitudes as a function of pressure. The best-linear-fit lines are shown for water and CO_2 separately and for the overall data set. The data are quite scattered, and the correlation coefficients, or R factors, are not particularly high. Nevertheless, during water injection and for the combined data, the correlation is significant at the 99% level. The correlation coefficient for CO_2 injection is poorer and lacks good statistical significance. From Figure 7, it appears that the events during CO_2 injection have slightly higher magnitudes than during water injection at the same pressures. Although no exact relationship should be inferred from these data,

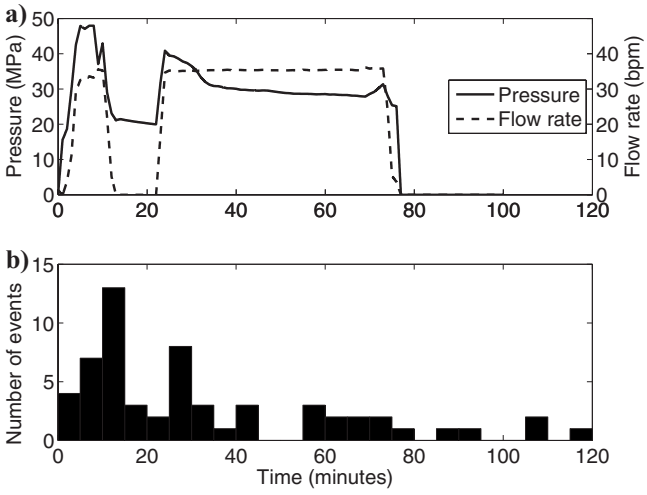

Figure 2. (a) Injection pressures (at surface) and flow rates during water injection. (b) Rate of microseismicity (bpm = barrels/minute).

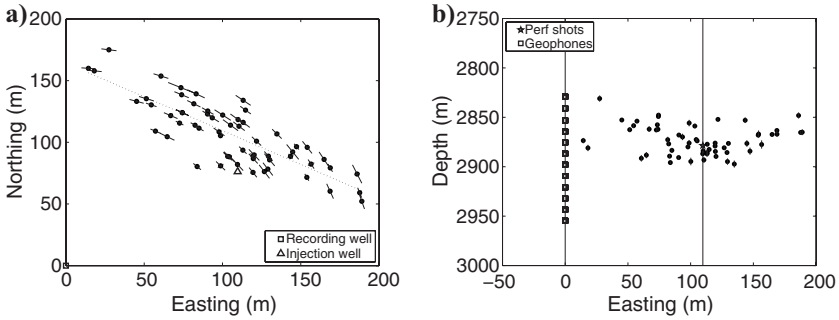

Figure 3. (a) Map and (b) cross-section views of event locations recorded during water injection. The location of the recording well is at (0,0), and the injection well is marked. Error bars represent the one-standard-deviation confidence interval (in some cases, these are smaller than the dots plotting the locations). The events are located northwest and southeast of the injection well, along a strike of ~120°, and in cross section are close to the injection depth.

we suggest that larger event magnitudes should be expected during periods of higher injection pressures, regardless of the compressibility of the injection fluid.

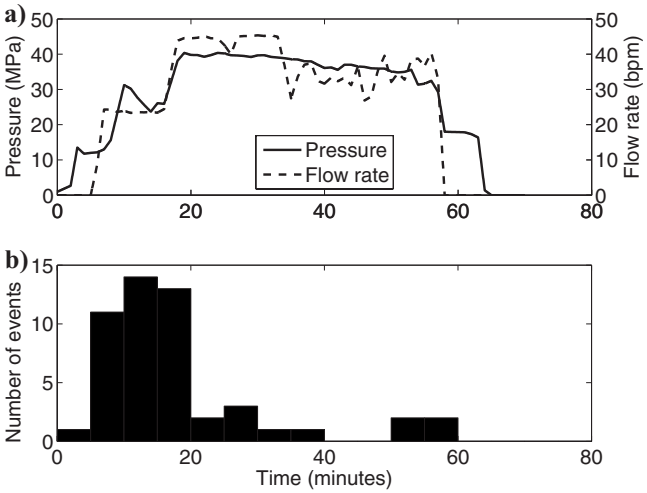

Figure 4. (a) Surface injection pressures and flow rates during CO_2 injection. (b) Rate of microseismicity (bpm = barrels/minute).

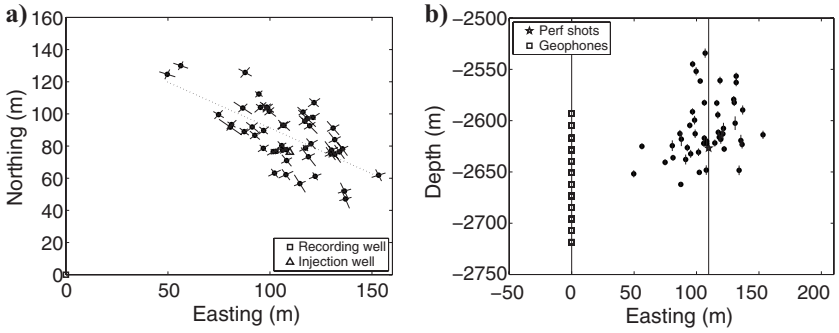

Figure 5. (a) Map and (b) cross-section views of event locations recorded during CO_2 injection. The recording well is at (0,0) and the injection well is marked. The error bars indicate the one-standard-deviation confidence interval. The events are located to the northwest and southeast of the injection point and in cross section extend well above the injection point.

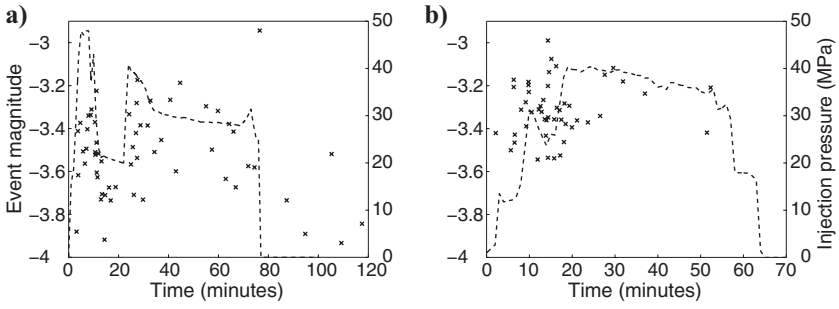

Figure 6. Surface injection pressures (dotted line) and event magnitudes (crosses) through time for (a) water and (b) CO_2 injection. There appears to be correlation between event magnitudes and injection pressures during both stages. Injection pressures and event magnitudes are similar for both stages.

We have noted some differences between water and CO_2 injection. We also note a greater temporal spread of events during water injection, whereas most events during CO_2 injection occur during the first 25 minutes. However, the most striking observation is the similarity of the response from the two fluids. The injection rates and pressures used during both stages are similar, and the result is that event magnitudes and rates of seismicity are also similar. There is certainly no evidence to suggest that CO_2 — the softer hammer — induces less seismicity than water.

SHEAR-WAVE SPLITTING

An alternative method of estimating the degree of fracturing is to use seismic anisotropy. Seismic anisotropy is defined as where the velocity of a seismic wave is dependent on its direction of travel and/or polarization. Seismic anisotropy can have many causes, but the most significant in hydrocarbon settings are horizontally aligned minerals (e.g., Valcke et al., 2006), horizontally aligned sedimentary fabrics (e.g., Hall et al., 2008), and vertically aligned fractures (e.g., Hudson, 1981), all of which can be modulated by stress (e.g., Zatsepin and Crampin, 1997; Verdon et al., 2008a). Detecting seismic anisotropy in the subsurface can identify sets of aligned fractures such as those generated during hydraulic fracture.

The most direct indicator of seismic anisotropy is shear-wave splitting. When a shear wave enters an anisotropic region, it is split into two orthogonally polarized waves, one of which travels faster than the other. The faster wave will arrive earlier at the geophone. By measuring the polarization of this S-wave (ψ) as well as the time lag between the fast and slow wave arrivals (δt), it is possible to characterize the anisotropy along a raypath. Usually, δt is normalized by the path length to give the percentage difference between fast and slow S-wave velocities δV_S. By considering the anisotropy along many raypaths, we can characterize the overall anisotropy of the rock.

The contribution of fractures and sedimentary fabrics to the overall anisotropic symmetry is nontrivial. However, by forward modeling using rock-physics theory, it is possible to invert shear-wave-splitting measurements for rock-physics properties such as vertical transversely isotropic (VTI) fabric strength, strike of vertically aligned fractures, and fracture density (Verdon et al., 2009). By measuring the splitting of shear waves recorded during both stages and inverting them for fracture density, we have an alternative way of comparing the amount of damage caused by CO_2 and water injection.

We measure the shear-wave splitting of both data sets using the semiautomated covariance matrix minimization approach of Teanby et al. (2004b), computing ψ and δt for each S-wave arrival at each geophone. Of the 780 potential splitting measurements during water injection (65 events × 12 geophones), 45 were deemed to pass the highest level of quality-control requirements outlined by Teanby et al. (2004b). Of the 600 potential measurements during CO_2 injection (50 events × 12 geophones), 47 were of the most reli-

able class. This is a reasonable success rate for a typical microseismic data set (Anboori et al.,2005). Cylindrical projections (e.g., Liu et al., 1989) of the splitting measurements are plotted in Figure 8.

We invert the shear-wave-splitting measurements, assuming the presence of a VTI sedimentary fabric with shear-wave-splittingmagnitude given by Thomsen's (1986) γ parameter. Verdon et al. (2009)show that the other Thomsen parameters (δ and ε) do not influence the splitting of subhorizontally traveling S-waves. The sedimentary fabric is superimposed with vertically aligned fractures, with nondimensional density ξ (as defined by Hudson, 1981) and strike α. We compute the rms misfit between observed and modeled splitting measurements, and we select the model that minimizes misfit as the most appropriate. The results of the inversion — the rms misfit as a function of γ, ξ, and α — are plotted in Figure 9 for water and in Figure 10 for CO_2. The best-fit values are $\gamma = 0.040$, $\xi = 0.104$, and $\alpha = 120°$ for water and $\gamma = 0.038$, $\xi = 0.012$, and $\alpha = 141°$ for CO_2. We plot cylindrical projections of the modeled splitting from the best-fit models in Figure 8 and note good agreement between observed and modeled values. Furthermore, the modeled fracture strikes match the fracture strikes inferred from event locations, indicating the success of the inversion.

The fracture strike appears to be poorly constrained for the CO_2 injection case. This is because when there are few fractures, their strike is unimportant. However, considering the 90% confidence ellipse in Figure 10, it is clear that for fracture densities above approximately 0.01 the possible fracture strikes center on 140°, becoming increasingly well constrained as fracture density increases. The estimates for γ are similar for both stages, which is encouraging. Kendall et al. (2007) note that the strength of VTI fabric (given by γ) often correlates with reservoir quality because the presence of clay particles reduces reservoir quality and introduces VTI symmetry. Given that the lithologies at the two depths are similar, we would expect to see similar-strength VTI fabrics in both cases, as is observed. The fracture densities recovered represent an average over the raypath. In reality, fractures are likely to be concentrated near the injector, meaning that what we have measured actually represents a lower bound for fracture density around the injection well.

Because the geophones have been placed at similar depths to the injection points, the S-waves used in this analysis have traveled subhorizontally at azimuths close to the fracture normals. Synthetic modeling (Verdon et al., 2009) suggests that such waves will be able to resolve the fracture strike and γ but will not provide good resolution for fracture density ξ. This is borne out in the results, with ξ being poorly resolved for both stages. At face value, fracture density appears to be higher during water injection. However, there is overlap between the 90% confidence intervals for the two stages. We conclude that although shear-wave splitting successfully images the fracture strike, the limitations of geophone geometry mean that shear-wave splitting is unable to provide the evidence to make a robust conclusion about the difference in fracture density between the two stages.

Synthetic inversions (Verdon et al., 2009) suggest that for shear-wave-splitting measurements to resolve fracture density, the geophones must be placed such that the S-waves have traveled at a more oblique angle to the fractures. This improvement could have been achieved in Weyburn by having a greater vertical spacing between geophones, by placing geophones above the point of injection, or by siting geophones in a well with an azimuth to the injection well that is not close to the minimum principal stress direction.

Table 1. Correlation coefficients *R* and statistical significance of correlation *P* for event magnitudes versus both injection pressure. We consider the data for both fluids separately, and the overall data set combined.

Fluid	*R*	*P* %
Water	0.422	99.9
CO_2	0.124	60.0
Combined	0.260	99.3

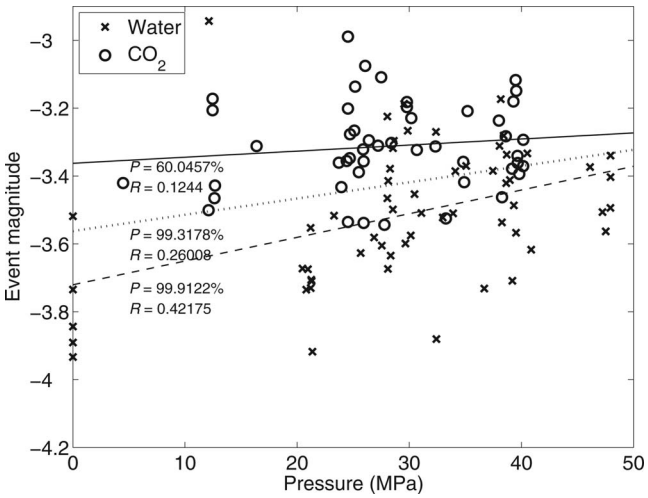

Figure 7. Event magnitudes as a function of the pressure when the event occurs. The events during water injection are marked by crosses; those during CO_2 are marked by open circles. The best-fit lines (dashed = water, solid = CO_2, dotted = combined), correlation coefficients, and statistical significances are marked.

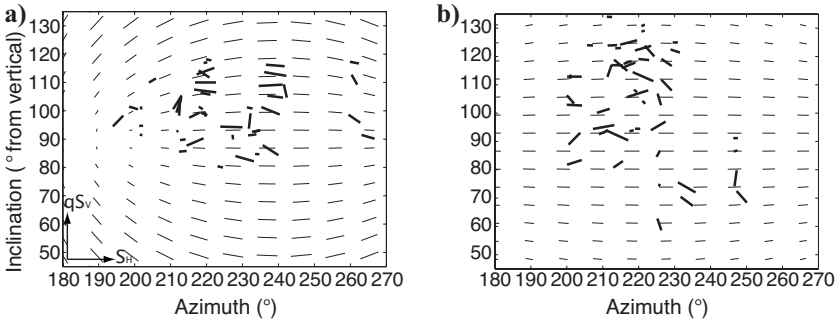

Figure 8. Cylindrical projections of splitting measurements (thicker ticks) for (a) water and (b) CO_2 injection. The *x*- and *y*-axes give the arrival angles of the S-waves used to measure splitting. The tick orientations indicate the fast splitting direction ψ. A vertical tick indicates ψ is parallel to the quasi-vertical S-wave direction qS_V, and a horizontal tick indicates ψ is horizontal (S_H). Tick lengths represent the percentage difference in speed of the fast and slow S-waves, or δV_S. Also plotted with thinner ticks are the results for the best-fit models in the same format as the observed data.

DISCUSSION

An understanding of the amount of fracturing that CO_2 injection is likely to induce is crucial in guaranteeing the security of any CCS project. It is also important in determining the feasibility of passive seismic monitoring tools. Of all active large-scale CCS projects, only Weyburn includes induced microseismic event detection in the monitoring program. The results from Weyburn indicate a low rate of microseismicity (Maxwell et al., 2004; White, 2008). Numerous reasons have been forwarded for the low activity rates, some based on the geomechanical properties of the reservoir (e.g., Jimenez et al., 2004) and some based on the fact that the geometry of the Weyburn reservoir makes it unlikely to fracture (e.g., Verdon et al., 2008b). An alternative explanation is that the higher compressibility of CO_2 might make it less likely to generate microseismic events.

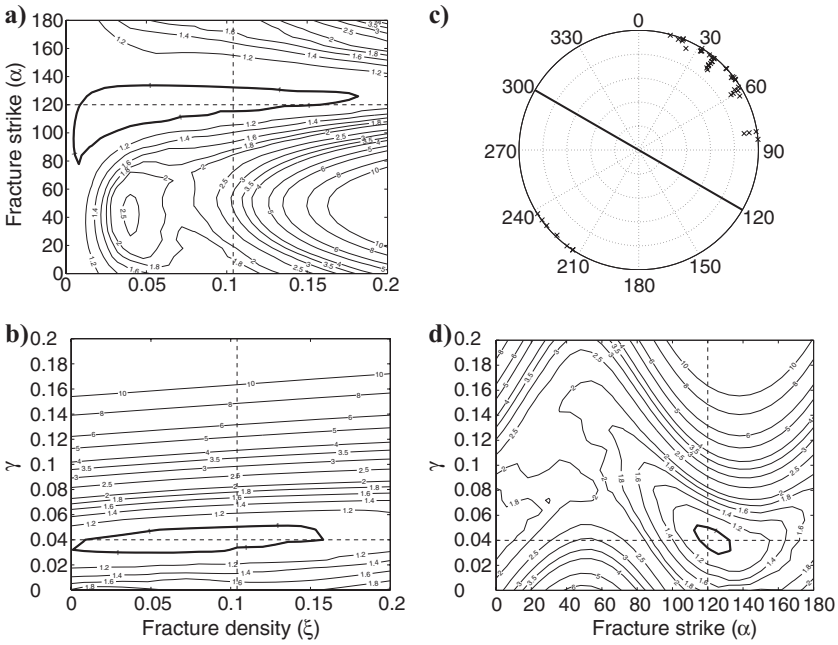

Figure 9. Shear-wave-splitting inversion results for water injection. (a) The normalized misfit contours as a function of ξ (fracture density) and α (fracture strike) at the best-fit γ (VTI fabric strength). A stereoplot of arrival angles is shown in (b) along with the strike of the vertical fracture set. The misfit as a function of ξ and γ at best-fit α is plotted in (c), and (d) shows γ and α at best-fit ξ. The dashed lines indicate the best-fit inversion results. The misfit contours are normalized such that value of 1 is the 90% confidence limit. The fracture strike and γ are well constrained; the fracture density is less so.

The data presented in our paper come from a hydraulic fracture job, where fluids have been injected at pressures greater than 40 MPa to induce fracturing; at Weyburn, injection pressures are 20–25 MPa to minimize fracturing. There are also differences in geology between Weyburn and the case we presented. As such, direct comparisons cannot be made. Nevertheless, in at least one case, CO_2 generated a pattern of seismicity similar to water. It remains a reasonable question whether the similarities between CO_2 and water that we observed will appear at the lower pressures and more stable injection regime of a CCS project. Although geomechanical simulation will undoubtedly contribute to this issue, a conclusive answer will probably be found only when further large-scale CCS projects are commissioned.

CONCLUSIONS

Alternative fluids continue to be used to induce hydraulic fracture, so it is of interest to compare the amount of deformation that they can induce. We have compared passive seismic monitoring results for a water-based gel and supercritical CO_2 injection in very similar conditions. The event locations show similar patterns during the two injection stages, imaging the formation of vertical fractures whose normals are parallel to the direction of minimum horizontal stress. The fractures formed during water injection extend further laterally, yet there are events found well above the injection depth during CO_2 injection, suggesting that its greater buoyancy has enabled CO_2 to migrate vertically. The events induced by the two fluids are of similar magnitudes and occur at similar rates. There is certainly no evidence to suggest that the softer fluid, CO_2, induces less deformation than water. We find instead that the event magnitudes correlate with injection pressures.

We have also used shear-wave splitting to image the fractures. Although at face value the water stage appears to have a higher fracture density, the geometry of event locations and geophones

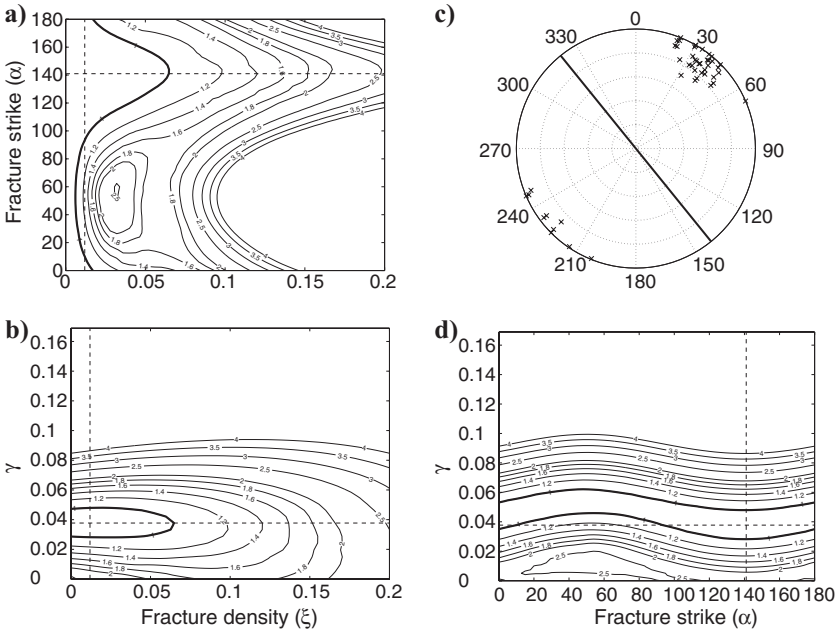

Figure 10. Shear-wave-splitting inversion results for CO_2 injection in the same format as Figure 9. Although the fracture density is less than for water injection (Figure 9), there is overlap between the 90% confidence intervals.

has made it difficult for splitting measurements to provide good constraints, so this conclusion is not robust.

We conclude that, despite the differences in compressibility, viscosity, density, and relative permeability between the fluids, CO_2 and water have similar induced patterns of microseismicity. This means that much of the abundant experience relating to water injection can be applied to CO_2 injection.

ACKNOWLEDGMENTS

The authors would like to thank Pinnacle Technologies Ltd. for making the microseismic data available, and Natalia Verkhovtseva for her help in the initial processing of the data. James Verdon was funded by a U. K. Energy Research Center (UKERC) Interdisciplinary Studentship. The authors would also like to thank the editors and reviewers whose comments have improved the quality of this work.

REFERENCES

Anboori, A., J.-M. Kendall, D. Raymer, and R. Jones, 2005, Microseismic monitoring and spatial variations in anisotropy — An example from Oman: 67th Annual Conference and Technical Exhibition, EAGE, Extended Abstracts, P094.

De Meersman, K., M. van der Baan, and J.-M. Kendall, 2006, Signal extraction and automated polarization analysis of multicomponent array data: Bulletin of the Seismological Society of America, **96**, 2415–2430.

Eisner, L., P. M. Duncan, W. M. Heigl, and W. R. Keller, 2009, Uncertainties in passive seismic monitoring: The Leading Edge, **28**, 648–655.

Hall, S. A., J.-M. Kendall, J. Maddock, and Q. Fisher, 2008, Crack density tensor inversion for analysis of changes in rock frame architecture: Geophysical Journal International, **173**, 577–592.

Hudson, J., 1981, Wave speeds and attenuation of elastic waves in material containing cracks: Geophysical Journal of the Royal Astronomical Society, **64**, 133–150.

Jimenez, J. A., R. J. Chalaturnyk, S. G. Whittaker, and G. Burrowes, 2004, A mechanical earth model for the Weyburn CO_2 monitoring and storage project and its relevance to long-term performance assessment: Proceedings of the 7th International Conference on Greenhouse Gas Control Technologies.

Kendall, J.-M., Q. J. Fisher, S. Covey Crump, J. Maddock, A. Carter, S. A. Hall, J. Wookey, S. Valcke, M. Casey, G. Lloyd, and W. Ben Ismail, 2007, Seismic anisotropy as an indicator of reservoir quality of siliclastic rocks, *in* S. Jolley, D. Barr, J. Walsh, and R. Knipe, eds., Structurally complex reservoirs: Geological Society of London Special Publication 292, 123–136.

Liu, E., S. Crampin, and D. C. Booth, 1989, Shear-wave splitting in cross-hole surveys: Modeling: Geophysics, **54**, 57–65.

Maxwell, S. C., J. Shemeta, E. Campbell, and D. Quirk, 2008, Microseismic deformation rate monitoring: Annual Technical Conference and Exhibition, Society of Petroleum Engineers, SPE 116596.

Maxwell, S. C., D. J. White, and H. Fabriol, 2004, Passive seismic imaging of CO_2 sequestration at Weyburn: 74th Annual International Meeting, SEG, Expanded Abstracts, 568–571.

Rutledge, J., W. Phillips, and M. Mayerhofer, 2004, Faulting induced by forced fluid injection and fluid flow forced by faulting: An interpretation of hydraulic fracture microseismicity, Carthage Cotton Valley gas field, Texas: Bulletin of the Seismological Society of America, **94**, 1817–1830.

Sminchak, J., N. Gupta, C. Byrer, and P. Bergman, 2002, Issues related to seismic activity induced by the injection of CO_2 in deep saline aquifers: Journal of Energy and Environmental Research, **2**, 32–46.

Teanby, N., J.-M. Kendall, R. H. Jones, and O. Barkved, 2004a, Stress-induced temporal variations in seismic anisotropy observed in microseismic data: Geophysical Journal International, **156**, 459–466.

Teanby, N., J.-M. Kendall, and M. van der Baan, 2004b, Automation of shear-wave splitting measurements using cluster analysis: Bulletin of the Seismological Society of America, **94**, 453–463.

Thomsen, L., 1986, Weak elastic anisotropy: Geophysics, **51**, 1954–1966.

Valcke, S. L. A., M. Casey, G. E. Lloyd, J.-M. Kendall, and Q. J. Fisher, 2006, Lattice preferred orientation and seismic anisotropy in sedimentary rocks: Geophysical Journal International, **166**, 652–666.

Verdon, J. P., D. A. Angus, J.-M. Kendall, and S. A. Hall, 2008a, The effects of microstructure and nonlinear stress on anisotropic seismic velocities: Geophysics, **73**, no. 4, D41–D51.

Verdon, J. P., D. A. Angus, J.-M. Kendall, J. Segura, S. Skachkov, and Q. J. Fisher, 2008b, The effects of geomechanical deformation on seismic monitoring of CO_2 sequestration: 78th Annual International Meeting, SEG, Expanded Abstracts, 2869–2873.

Verdon, J. P., J. M. Kendall, and A. Wüstefeld, 2009, Imaging fractures and sedimentary fabrics using shear wave splitting measurements made on passive seismic data: Geophysical Journal International, **179**, 1245–1254.

White, D. J., 2008, Geophysical monitoring in the IEA GHG Weyburn-Midale CO_2 monitoring and storage project: 78th Annual International Meeting, SEG, Expanded Abstracts, 2846–2849.

Zatsepin, S., and S. Crampin, 1997, Modelling the compliance of crustal rock — I. Response of shear-wave splitting to differential stress: Geophysical Journal International, **129**, 477–494.

Zimmer, U., S. Maxwell, C. Waltman, and N. Warpinski, 2007, Microseismic monitoring quality-control (QC) reports as an interpretative tool for non-specialists: Annual Technical Conference and Exhibition, Society of Petroleum Engineers, SPE 110517.